Supplementary information for: Single-Chain Magnet Behavior in a Finite Linear Hexanuclear Molecule

Authors

Felix Houard,[a] Frederic Gendron,[a] Yan Suffren,[a] Thierry Guizouarn,[a] Vincent Dorcet,[a] Guillaume Calvez,[a] Carole Daiguebonne,[a] Olivier Guillou,[a] Boris Le Guennic,[a] Matteo Mannini,[b] Kevin Bernot*[a,c]

Affiliations

[a] Univ Rennes, INSA Rennes, CNRS, ISCR (Institut des Sciences Chimiques de Rennes), UMR 6226, F 35000 Rennes, FRANCE.
[b] LAboratory for Molecular Magnetism (LA.M.M.), Dipartimento di Chimica "Ugo Schiff", Università degli Studi di Firenze (DICUS), INSTM, UdR Firenze, Via della Lastruccia n. 3, Sesto Fiorentino (FI) 50019 ITALY.
[C] Institut Universitaire de France, 1 rue Descartes, 75005, Paris, FRANCE.

Experimental section:

1. Synthesis $[(Tb(hfac)_3)_6(NITPhOHexyl)_5(H_2O)_2]\bullet CHCl_3.C_7H_{16}$, "*hexanuclears*"

All chemicals and solvents used are commercially available, of reagent grade and used without further purification. The synthesis of the 2-(4'-(hexyloxy)phenyl)-4,4,5,5-tetramethylimidazolin-1-oxyl-3-oxide (abbrev. NIT-Ph-O-Hexyl) is reported elsewhere.[1] 40.8 mg of terbium hexafluoroacetylacetonate dihydrate (abbrev. $Tb(hfac)_3{\cdot}2H_2O$) (0.05 mmol) was dissolved in 40 mL of boiling n-heptane, then concentrated until the volume reaches 10 mL. 16.7 mg (0.05 mmol, 1 eq.) of NIT-Ph-O-Hexyl radical dissolved in $CHCl_3$ (7 mL) was added and the solution was allowed to cool at room temperature. The final solution was filtered and kept under evaporation in a sealed dessicator whose bottom was filled with a layer of water, giving green platelets after few days. Yield: 42%. Elemental analysis (%) calcd. for $Tb_6C_{193}H_{184}N_{10}O_{53}F_{108}Cl_3$: C 35.10; H 2.81; N 2.12. Found: C 37.42; H 3.11; N 2.63.

2. Powder X-Ray diffraction

Experimental diffraction patterns have been collected with a Panalytical X'pert Pro diffractometer, equipped with a X'Celerator detector. Typical recording conditions were

45 kV, 40 mA for CuK_α (λ = 1.542 Å) in θ/θ mode. Simulated pattern was calculated thank to the Mercury 2020.1 program from CCDC.

3. Crystal structure determination

Fresh single crystals of *hexanuclears* were mounted on a D8 VENTURE Bruker AXS diffractometer equipped with a (CMOS) PHOTON 100 detector. Crystal data collection was performed with Mo$K\alpha$ radiation (λ = 0.70713 Å) at 150 K. The structure was solved by dual-space algorithm using the SHELXT program[1], and then refined with full-matrix least-squares methods based on F2 (SHELXL)[2]. The contribution of the disordered solvents to the calculated structure factors was estimated following the BYPASS algorithm[3], implemented as the SQUEEZE option in PLATON[4]. A new data set, free of solvent contribution, was then used in the final refinement. All non-hydrogen atoms were refined with anisotropic atomic displacement parameters. H atoms were finally included in their calculated positions and treated as riding on their parent atom with constrained thermal parameters. A final refinement on F^2 with 59734 unique intensities and 3379 parameters converged at ωRF_2 = 0.1039 (RF_1 = 0.0472) for 44434 observed reflections with I > 2σ(I).

Supplementary crystallographic data can be obtained free of charge from the Cambridge Crystallographic Data Centre (CDCC) under the deposition number CCDC-2076378.

4. Thermogravimetric studies

Thermogravimetric and thermodifferential (TGA/TDA) analyses were performed with a Perkin-Elmer Pyris Diamond analyzer in a platinum crucible between room temperature and 950°C under N_2 atmosphere with a heating rate of 5°C. min^{-1}. The compound was maintained at 1000°C under air atmosphere for one hour to insure complete combustion.

5. FTIR studies

FTIR studies were performed with a Perkin Elmer Frontier UATR spectrometer on as synthesized powders (from 4000 to 550 cm^{-1}, res. 1 cm^{-1}).

STA-coupled FTIR studies were performed in a ceramic crucible between room temperature and 950°C under N_2 atmosphere with the same spectrometer (from 4000 to 450cm^{-1}, res. 2cm^{-1}), coupled to a Perkin Elmer Simultaneous Thermal Analyzer STA6000 at an heating rate of 20°C min^{-1} thanks to a Perkin Elmer Transfer Line TL8000.

6. SEM measurements

Measurements were performed at room temperature with a Hitachi TM-1000 benchtop microscope (Hitachi High-Technologies, Corporation Tokyo Japan), equipped with a silicon drift detector with an energy resolution of 165 eV and an EDS analysis system (SwiftED-TM,

Oxford Instruments, Link INCA). Samples were stuck on a graphite stub fixed at 7 mm from the beam and observed with a 15 kV accelerated electron beam under high vacuum.

7. Luminescence measurements

The solid excitation and emission spectra were measured using a Horiba Jobin-Yvon Fluorolog-III spectrofluorimeter, equipped with a double grating excitation and emission monochromator with dispersions of 2.1 nm/mm (1200 grooves/mm). The steady-state luminescence was excited by unpolarized light from a 450 W xenon CW lamp and detected at a 90° angle by a UV-Visible-nearIR Hamamatsu R928 photomultiplier tube (sensitivity 190 - 860 nm). Spectra were reference corrected for both the excitation source light intensity variation (lamp and grating) and the emission spectral response (detector and grating). Appropriate filters were used to remove the residual excitation laser light, the Rayleigh scattered light and associated harmonics from spectra. The excitation/emission spectra recordings were realized on powder sample placed directly into quartz cuvette and cooled in an optical cryostat capable of reaching temperature down to 77 K through a continuous nitrogen liquid flow and a nitrogen atmosphere inside the sample chamber (OptistatCF, Oxford Inst.).

8. Specific heat measurements

Specific heat capacity was measured with a Quantum Design PPMS between 2 and 200 K on microcrystalline powder pressed in pellet, with a layer of Apiezon M grease to ensure sufficient thermal contact between the puck and the sample.

9. Magnetic measurements

Magnetic studies were performed using a MPMS SQUID magnetometer equipped with a RSO probe and a ^{3}He insert for hysteresis measurements below 1.5 K (field sweep rate was 15.5 Oe.s^{-1}). Polycrystalline samples were pressed into pellets to avoid in-field crystallite orientation. Samples were inserted at 100K in the magnetometer. Measurements corrected from diamagnetic contributions as calculated with Pascal's constants.

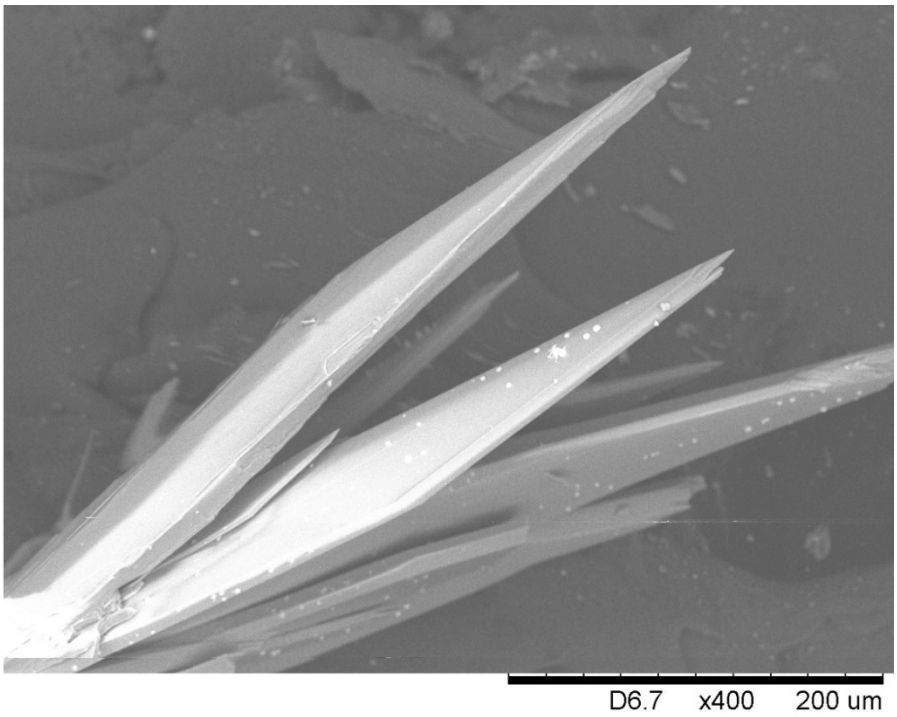

Figure S1: Scanning Electron Microscope image of crystals of *hexanuclears* (magnification x400).

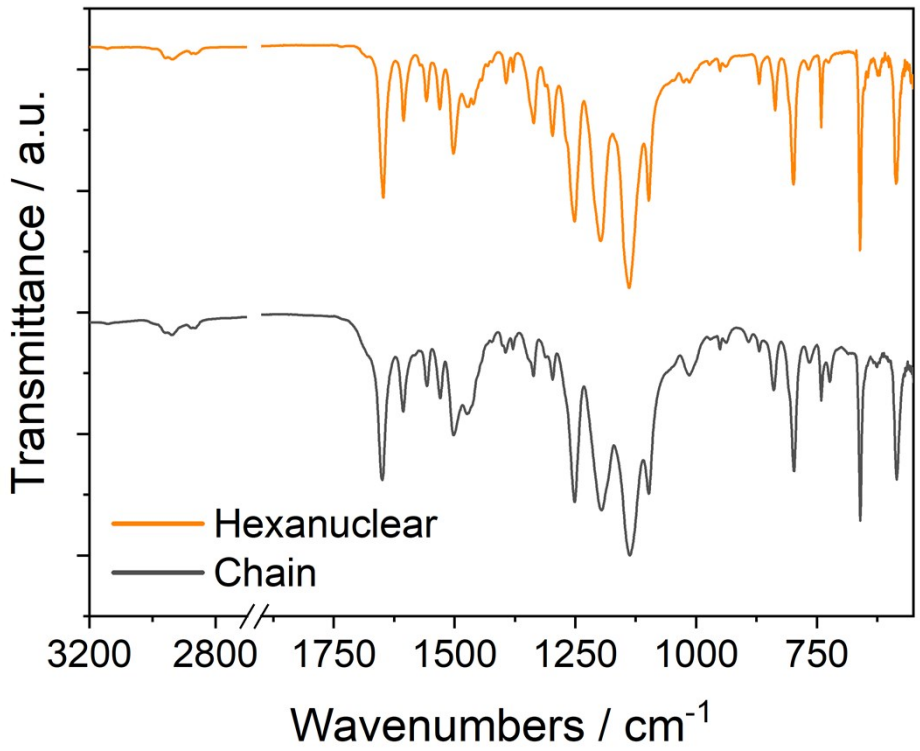

Figure S2. FTIR spectra of *chains* and *hexanuclears*.

Main vibrational bands (cm^{-1}): 2957 (w), 2954(w), 2950 (w), 2936 (w), 2878 (w), 2871 and 2864 (w) *ν*(C-H), 1648 (s, *ν*(C=C)), 1605 (m, *ν*(C=C_{arom})), 1501 (m, *ν*(C=C)), 1336 (w, *ν*(N-O)), 1296 (w, *ν*(C-O)), 1253 (s, *ν*(C_{arom}-O in ether, C-F), 1195 (s, *ν*(C-O, C-F)), 1139 (s, *ν*(C-N)).

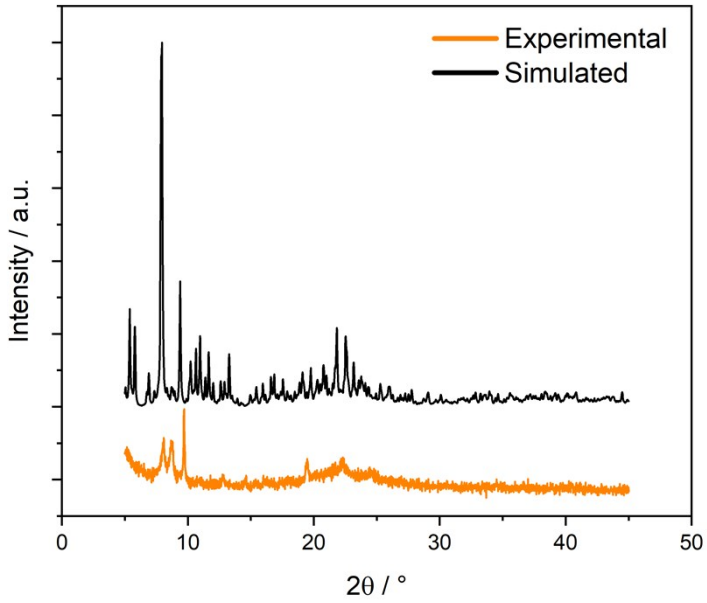

Figure S3. Experimental (blue) and simulated (black) *hexanuclears* powder X-Ray diffraction patterns highlighting the quick amorphization of the powder during the sample preparation.

Table S1: Main crystallographic parameters for the *hexanuclears*.

Chemical name	$[(Tb(hfac)_3)_6(NITPhOHexyl)_5(H_2O)_2]\bullet CHCl_3.C_7H_{16}$
Abbreviation	**hexanuclears**
Formula	$Tb_6C_{193}H_{184}N_{10}O_{53}F_{108}Cl_3$
***M* (g.mol^{-1})**	6603.36
Crystal system	Monoclinic
Space group	$P2_1/n$ (N°14)
***a* (Å)**	27.995(4)
***b* (Å)**	22.437(3)
***c* (Å)**	41.691(5)
***α* [°]**	90
***β* [°]**	94.178(4)
***γ* [°]**	90
***V* [Å^3]**	26118
Z	4
***T* (K)**	150
***2ϑ* range**	2.3867–27.4754
Reflns collected	262314
Indep. reflns	59734

Obs. reflns	44434
Parameters	3379
R_1 **[** $I > 2\sigma(I)$**]** wR_2 **[** $I > 2\sigma(I)$**]**	4.72 10.39
GOF	1.017

R_1 defined as $\sum(|F_0| - |F_c|)/\sum|F_0|$

R_2 defined as $\sqrt{\sum w(|F_0|^2 - |F_c|^2)^2/\sum w(|F_0|^2)^2}$

Table S2. Main bond distances (Å) and angles (°) for *hexanuclears.*

Tb1		**Tb2**		**Tb3**	
Tb1-O1	2.407	Tb2-O10	2.401	Tb3-O19	2.364
Tb1-O2	2.380	Tb2-O11	2.365	Tb3-O20	2.346
Tb1-O3	2.349	Tb2-O12	2.344	Tb3-O21	2.362
Tb1-O4	2.337	Tb2-O13	2.340	Tb3-O22	2.363
Tb1-O5	2.338	Tb2-O14	2.366	Tb3-O23	2.331
Tb1-O6	2.356	Tb2-O15	2.384	Tb3-O24	2.343
Tb1-O7	2.386	Tb2-O16	2.346	Tb3-O25	2.345
Tb1-O8	2.371	Tb2-O17	2.389	Tb3-O26	2.379
O1-Tb1-O2	74.34	O10-Tb2-O11	149.75	O19-Tb3-O20	103.15
O1-Tb1-O3	78.59	O10-Tb2-O12	87.47	O19-Tb3-O21	74.65
O1-Tb1-O4	107.74	O10-Tb2-O13	72.03	O19-Tb3-O22	149.27
O1-Tb1-O5	70.79	O10-Tb2-O14	71.91	O19-Tb3-O23	91.74
O1-Tb1-O6	142.64	O10-Tb2-O15	73.22	O19-Tb3-O24	73.56
O1-Tb1-O7	82.14	O10-Tb2-O16	106.43	O19-Tb3-O25	72.88
O1-Tb1-O8	142.63	O10-Tb2-O17	135.77	O19-Tb3-O26	137.53
O2-Tb1-O3	72.29	O11-Tb2-O12	72.77	O20-Tb3-O21	72.60
O2-Tb1-O4	145.18	O11-Tb2-O13	122.89	O20-Tb3-O22	75.39
O2-Tb1-O5	135.89	O11-Tb2-O14	135.09	O20-Tb3-O23	139.08
O2-Tb1-O6	124.44	O11-Tb2-O15	78.91	O20-Tb3-O24	147.26
O2-Tb1-O7	75.64	O11-Tb2-O16	75.15	O20-Tb3-O25	74.55
O2-Tb1-O8	72.90	O11-Tb2-O17	73.94	O20-Tb3-O26	93.02
O3-Tb1-O4	74.15	O12-Tb2-O13	76.74	O21-Tb3-O22	75.74
O3-Tb1-O5	124.40	O12-Tb2-O14	147.80	O21-Tb3-O23	75.14
O3-Tb1-O6	135.28	O12-Tb2-O15	72.05	O21-Tb3-O24	133.94
O3-Tb1-O7	145.97	O12-Tb2-O16	135.45	O21-Tb3-O25	126.21
O3-Tb1-O8	74.75	O12-Tb2-O17	111.46	O21-Tb3-O26	147.73
O4-Tb1-O5	72.75	O13-Tb2-O14	73.53	O22-Tb3-O23	72.79
O4-Tb1-O6	75.73	O13-Tb2-O15	133.68	O22-Tb3-O24	124.06
O4-Tb1-O7	139.03	O13-Tb2-O16	147.71	O22-Tb3-O25	133.32

O4-Tb1-O8	89.66	O13-Tb2-O17	74.12	O22-Tb3-O26	72.66
O5-Tb1-O6	75.21	O14-Tb2-O15	122.15	O23-Tb3-O24	73.43
O5-Tb1-O7	73.60	O14-Tb2-O16	75.45	O23-Tb3-O25	146.23
O5-Tb1-O8	146.53	O14-Tb2-O17	71.80	O23-Tb3-O26	101.27
O6-Tb1-O7	73.74	O15-Tb2-O16	72.09	O24-Tb3-O25	73.41
O6-Tb1-O8	72.90	O15-Tb2-O17	149.67	O24-Tb3-O26	71.90
O7-Tb1-O8	106.37	O16-Tb2-O17	87.82	O25-Tb3-O26	74.16
Tb4		**Tb5**		**Tb6**	
Tb4-O28	2.371	Tb5-O37	2.374	Tb6-O46	2.391
Tb4-O29	2.367	Tb5-O38	2.329	Tb6-O47	2.360
Tb4-O30	2.364	Tb5-O39	2.347	Tb6-O48	2.395
Tb4-O31	2.365	Tb5-O40	2.376	Tb6-O49	2.371
Tb4-O32	2.325	Tb5-O41	2.338	Tb6-O50	2.350
Tb4-O33	2.373	Tb5-O42	2.359	Tb6-O51	2.325
Tb4-O34	2.345	Tb5-O43	2.363	Tb6-O52	2.357
Tb4-O35	2.388	Tb5-O44	2.385	Tb6-O53	2.411
O28-Tb4-O29	74.73	O37-Tb5-O38	105.53	O46-Tb6-O47	75.74
O28-Tb4-O30	71.52	O37-Tb5-O39	73.49	O46-Tb6-O48	72.17
O28-Tb4-O31	148.37	O37-Tb5-O40	148.62	O46-Tb6-O49	109.58
O28-Tb4-O32	93.83	O37-Tb5-O41	91.23	O46-Tb6-O50	73.72
O28-Tb4-O33	72.72	O37-Tb5-O42	71.64	O46-Tb6-O51	83.93
O28-Tb4-O34	104.02	O37-Tb5-O43	73.95	O46-Tb6-O52	143.79
O28-Tb4-O35	137.25	O37-Tb5-O44	136.99	O46-Tb6-O53	145.75
O29-Tb4-O30	73.02	O38-Tb5-O39	73.69	O47-Tb6-O48	71.72
O29-Tb4-O31	125.07	O38-Tb5-O40	73.50	O47-Tb6-O49	143.88
O29-Tb4-O32	73.22	O38-Tb5-O41	138.28	O47-Tb6-O50	138.59
O29-Tb4-O33	133.82	O38-Tb5-O42	73.32	O47-Tb6-O51	72.21
O29-Tb4-O34	147.24	O38-Tb5-O43	145.17	O47-Tb6-O52	120.19
O29-Tb4-O35	70.56	O38-Tb5-O44	89.11	O47-Tb6-O53	80.60
O30-Tb4-O31	134.24	O39-Tb5-O40	76.33	O48-Tb6-O49	76.12
O30-Tb4-O32	145.70	O39-Tb5-O41	75.10	O48-Tb6-O50	122.73
O30-Tb4-O33	124.16	O39-Tb5-O42	122.32	O48-Tb6-O51	140.52
O30-Tb4-O34	75.61	O39-Tb5-O43	135.31	O48-Tb6-O52	141.67
O30-Tb4-O35	75.04	O39-Tb5-O44	149.00	O48-Tb6-O53	77.12
O31-Tb4-O32	72.58	O40-Tb5-O41	72.74	O49-Tb6-O50	73.88
O31-Tb4-O33	76.41	O40-Tb5-O42	134.08	O49-Tb6-O51	142.76
O31-Tb4-O34	72.88	O40-Tb5-O43	125.06	O49-Tb6-O52	77.37
O31-Tb4-O35	74.08	O40-Tb5-O44	74.09	O49-Tb6-O53	76.58
O32-Tb4-O33	77.22	O41-Tb5-O42	148.14	O50-Tb6-O51	77.33
O32-Tb4-O34	138.68	O41-Tb5-O43	75.86	O50-Tb6-O52	74.53

O32-Tb4-O35	99.20	O41-Tb5-O44	104.36	O50-Tb6-O53	137.84
O33-Tb4-O34	73.22	O42-Tb5-O43	73.68	O51-Tb6-O52	72.52
O33-Tb4-O35	149.91	O42-Tb5-O44	74.54	O51-Tb6-O53	112.00
O34-Tb4-O35	92.47	O43-Tb5-O44	71.60	O52-Tb6-O53	70.14

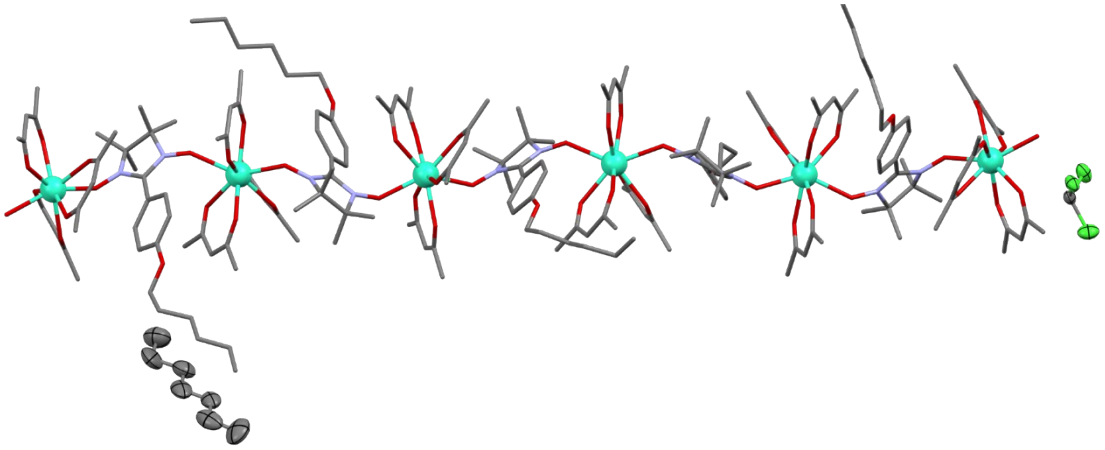

Figure S4. Representation of the asymmetric unit of the *hexanuclears*, including the heptane and chloroform crystallization solvents represented with their thermal ellipsoids (hydrogens and fluorine atoms of the hexanuclear molecule omitted for clarity).

Table S3. Continuous Shape Measurements (CShM)[5] for *hexanuclears*.

Coordination geometry (site symmetry)	Square antiprism (D_{4d})	Triangular dodecahedron (D_{2d})	Bi-augmented trigonal prism (C_{2v})
Tb1 CShM	**0.841**	**0.777**	1.795
Tb2 CShM	**0.891**	**0.825**	1.883
Tb3 CShM	1.577	**0.234**	2.076
Tb4 CShM	1.673	**0.265**	1.914
Tb5 CShM	1.173	**0.460**	1.973
Tb6 CShM	**0.412**	1.775	1.761

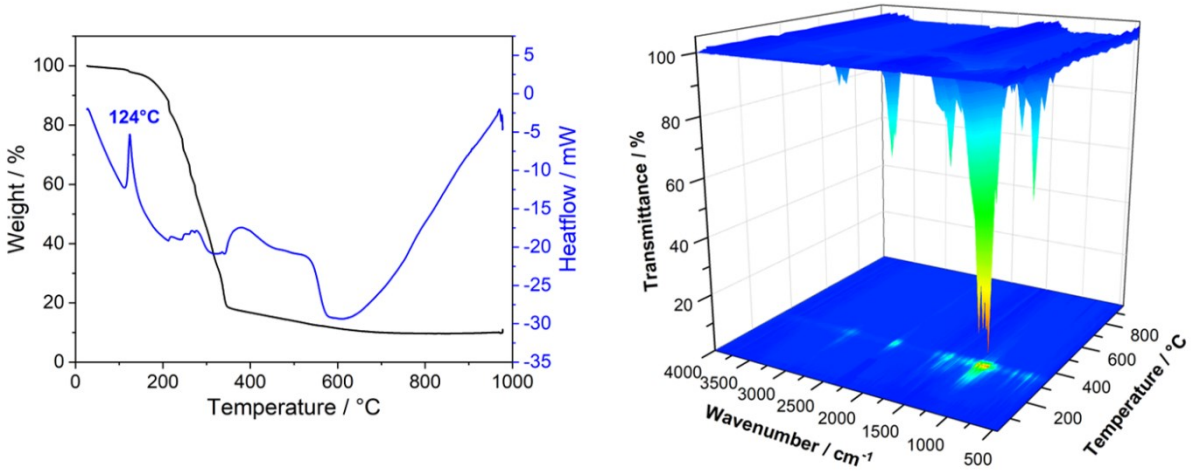

Figure S5. (Left) Thermogravimetric (TGA, black line) and thermodifferential analyses (DTA, blue line) of *hexanuclears*; (right) 3D plot of the FTIR analyses of the TGA/DTA exhaust gases.

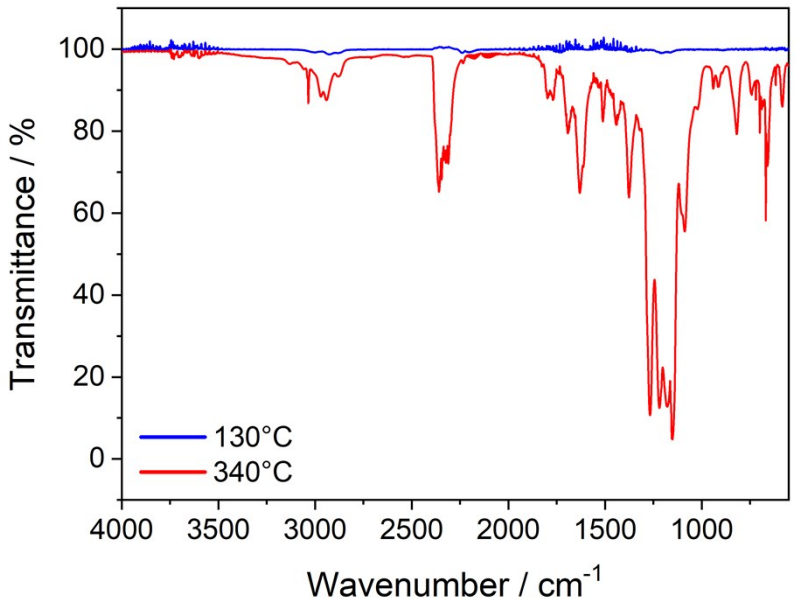

Figure S6: FTIR analyses of the TGA/DTA exhaust gases measured at 130°C and 340°C for *hexanuclears.*

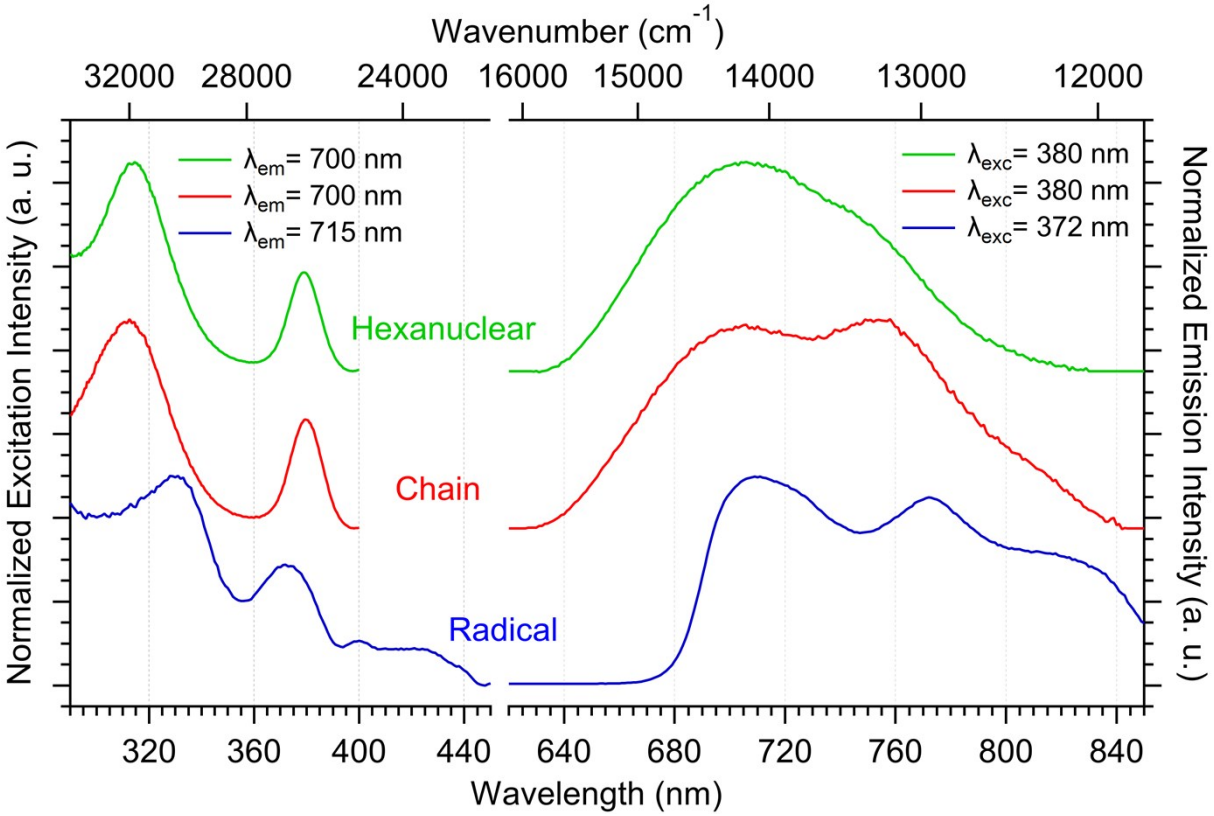

Figure S7: Normalized solid-state excitation and emission spectra at 77 K measured for the uncoordinated radical (blue), the *chains* (red) and the *hexanuclears* (green).

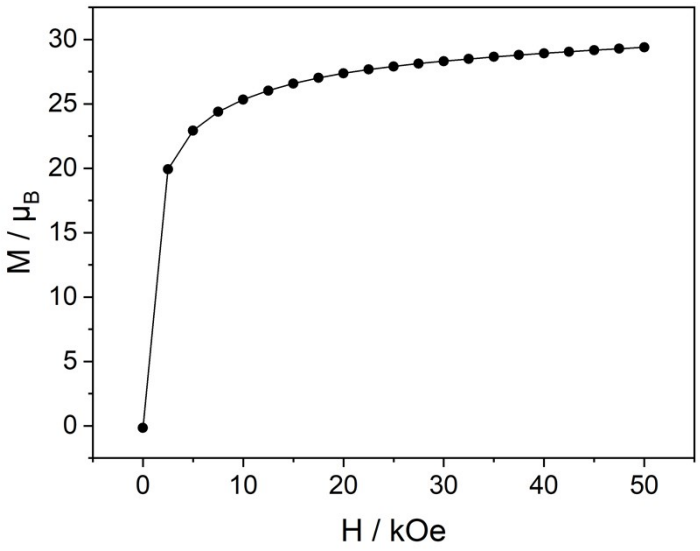

Figure S8. Magnetization versus field measurement at 2 K measured on pressed pellets of *hexanuclears.*

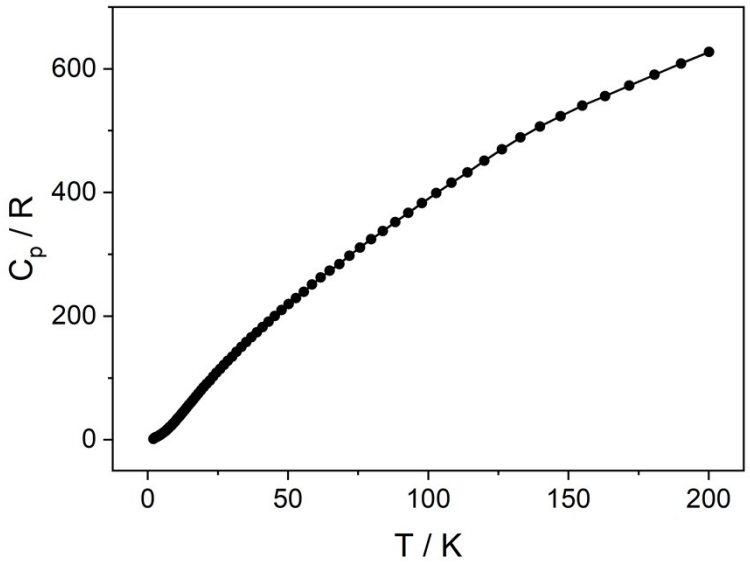

Figure S9. Specific heat measurement on pressed pellets of *hexanuclears.*

Theoretical calculations and computational details.

The calculations were performed on simplified structures of the *hexanuclears.* Experimentally, the hexanuclear corresponds to four $[Tb(hfac)_3(NIT\text{-}O\text{-}Hexyl)_2]$ and two $[Tb(hfac)_3(NIT\text{-}O\text{-}Hexyl)(H_2O)]$ molecular units exhibiting slightly different coordination sphere around the Tb^{3+} centers. In order to decrease the computational cost of the wavefunction theory (WFT) calculations, these experimental molecular units were represented by using model structures where the Hexyl chains are replaced by methyl groups, such as $[Tb(hfac)_3(NIT\text{-}O\text{-}CH_3)_2]$ and $[Tb(hfac)_3(NIT\text{-}O\text{-}CH_3)(H_2O)]$ (see top of Figure S8). To simplify the discussion, the six different models are labeled **$[Tb(1)\text{-}NIT_2]^{2-}$**, **$[Tb(2)\text{-}NIT_2]^{2-}$**, **$[Tb(3)\text{-}NIT_2]^{2-}$**, **$[Tb(4)\text{-}NIT_2]^{2-}$**, **$[Tb(5)\text{-}NIT\text{-}H_2O]^{-}$** and **$[Tb(6)\text{-}NIT\text{-}H_2O]^{-}$**, in the following. It is worth mentioning that the **$[Tb(5)\text{-}NIT\text{-}H_2O]^{-}$** and **$[Tb(6)\text{-}NIT\text{-}H_2O]^{-}$** units correspond to the extremities of the hexanuclear. Additionally, in order to evaluate the presence of magnetic interactions between the **TbNIT-Ph-O-Hexyl** hexanuclears, two dimer models were also investigated and are labelled **$[Dimer\text{-}Tb(1)]^{2-}$** and **$[Dimer\text{-}Tb(2)]^{2-}$**, respectively (see bottom of Figure S8).

The hydrogen atom positions of the model structures were optimized by using Kohn-Sham density functional theory (DFT) with the Amsterdam Density Functional (ADF[6-8]) software package. These calculations utilized the scalar all-electron zeroth-order regular approximation (ZORA[9]). The PBE[10] functional (Perdew-Burke-Ernzerhof) from the generalized gradient approximation, was employed along with the triple-ζ polarized Slater-type orbital (STO) all-electron basis set with two sets of polarization functions for all atoms (TZ2P[9]).

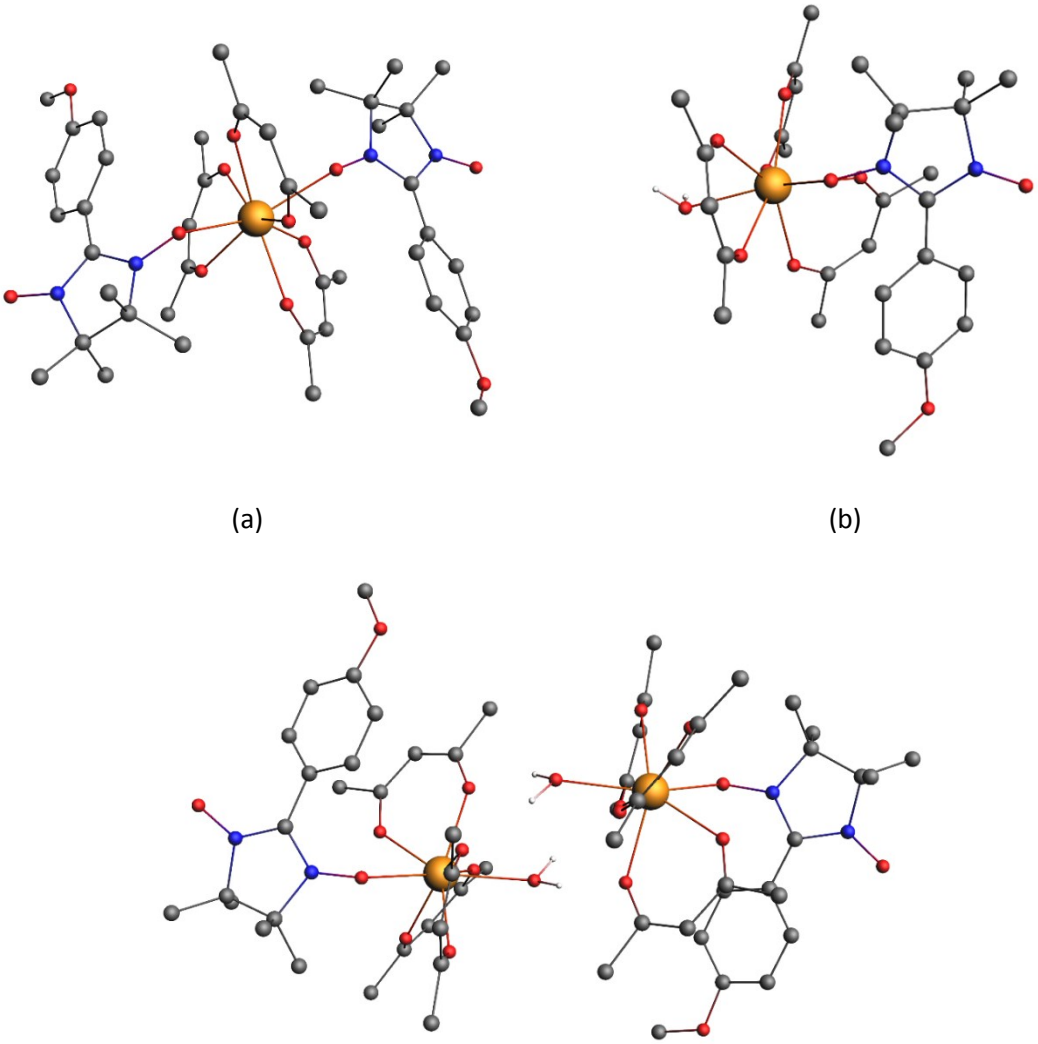

(a) (b)

(c)

Figure S10. Model compounds for $[Tb(1)\text{-}NIT_2]^{2-}$ (a), $[Tb(6)\text{-}NIT\text{-}H_2O]^{-}$ (b) and $[Dimer\text{-}Tb(1)]^{2-}$ (c).

The WFT calculations were performed with the help of the Molcas 8.2 software packages[11] on the di-anionic molecular units in order to obtain diamagnetic NIT ligands, and evaluate the magnetic properties arising from the Tb^{3+} centers only. In these calculations, the complete active space self-consistent field[12] (CASSCF) approach was used to treat the static correlation effects arising from the partially filled 4f shell of the Tb^{3+} ion. The second-order Douglas-Kroll-Hess[13-16] scalar relativistic (SR) Hamiltonian was used to treat the scalar relativistic effects in combination with the all-electron atomic natural orbital relativistically contracted (ANO-RCC) basis set from the Molcas library.[17-19] The basis sets were contracted to the triple-ζ plus polarization (TZP) quality for the Tb, N and O atoms (Tb = 25s22p15d11f4g2h/8s7p4d3f2g1h; N, O = 14s9p5d3f2g/4s3p2d1f), and to the double-ζ (DZ) quality for the H, C and F atoms (H = 8s4p3d1f/2s; C, F = 14s9p5d3f2g/3s2p). Additionally,

the C atoms between the two NO groups of each NIT radical ligands were treated with a basis set contracted to the TZP quality, whereas the O atoms not coordinated to the Tb centers were treated using a basis set contracted to DZ quality. The calculations employed the state-averaged formalism at the SR level by taking into account the 7 septet, the 140 quintet, 588 triplet and the 396 singlet spin states arising from the 8 electrons spanning the seven 4f orbitals (i.e. CAS(8,7)). The spin-orbit coupling (SOC) was then introduced within a state interaction among the basis of calculated SR states using the restricted active space state interaction (RASSI) approach.[20] Herein the SOC matrix is diagonalized using the calculated 7 SR septet, 140 SR quintet, the 91st lowest SR triplet and the 77th lowest SR singlet spin states. The EPR *g*-factors were calculated according to Ref. 21 as implemented in the RASSI module of Molcas, whereas the magnetic susceptibility and magnetization calculations were performed using the Single-Aniso and Poly-Anyso module of Molcas as detailed in Ref. 22.

Table S4. Calculated relative energies (ΔE in cm^{-1}) and EPR g-Factors for the lowest states deriving from the $^7F_6$ level of the Tb^{3+} ion in the three model compounds.

	[Tb(1)-NIT$_2$]$^{2-}$			**[Tb(2)-NIT$_2$]$^{2-}$**			**[Tb(3)-NIT$_2$]$^{2-}$**		
	ΔE	g∥	g⊥	ΔE	g∥	g⊥	ΔE	g∥	g⊥
GS	0	16.58	0.00	0	16.99	0.00	0	17.25	0.00
ES1	20	17.51	0.00	16	16.64	0.00	81	12.90	0.00
ES2	61	11.92	0.00	66	11.39	0.00	111	-	-
ES3	100	-	-	105	-	-	149	10.47	0.00
ES4	159	10.01	0.00	165	10.13	0.00	230	11.71	0.00
ES5	217	13.40	0.00	282	13.63	0.00	369	13.97	0.00
ES6	431	17.08	0.00	470	17.24	0.00	527	17.04	0.00
	[Tb(4)-NIT$_2$]$^{2-}$			**[Tb(5)-NIT-H$_2$O]$^{-}$**			**[Tb(6)-NIT-H$_2$O]$^{-}$**		
	ΔE	g∥	g⊥	ΔE	g∥	g⊥	ΔE	g∥	g⊥
GS	0	17.19	0.00	0	17.26	0.00	0	16.98	0.00
ES1	60	14.99	0.00	85	12.62	0.00	65	-	-
ES2	81	10.53	0.00	133	-	-	101	5.61	0.00
ES3	116	-	-	183	10.27	0.00	184	9.29	0.00
ES4	187	10.64	0.00	231	15.35	0.00	273	16.30	0.00
ES5	310	13.73	0.00	287	13.59	0.00	303	14.28	0.00
ES6	486	17.16	0.00	361	16.32	0.00	388	15.88	0.00

Table S5. Calculated M_J contributions (in per-cent) associated to the GS wave-functions for the model compounds.

	|±6>	|±5>	|±4>	|±3>	|±2>	|±1>	|0>
[Tb(1)-NIT$_2$]$^{2-}$	76.4	5.8	14.8	1.6	0.8	0.2	0.6
[Tb(2)-NIT$_2$]$^{2-}$	84.4	2.4	10.6	0.8	1.4	0.4	0.1
[Tb(3)-NIT$_2$]$^{2-}$	90.0	0.2	7.6	0.2	1.4	0.4	0.3
[Tb(4)-NIT$_2$]$^{2-}$	88.8	0.2	8.6	0.2	1.4	0.4	0.4
[Tb(5)-NIT-H$_2$O]$^{-}$	90.6	0.0	6.4	0.6	2.0	0.0	0.3
[Tb(6)-NIT-H$_2$O]$^{-}$	87.0	0.0	8.4	0.2	3.4	0.0	1.0

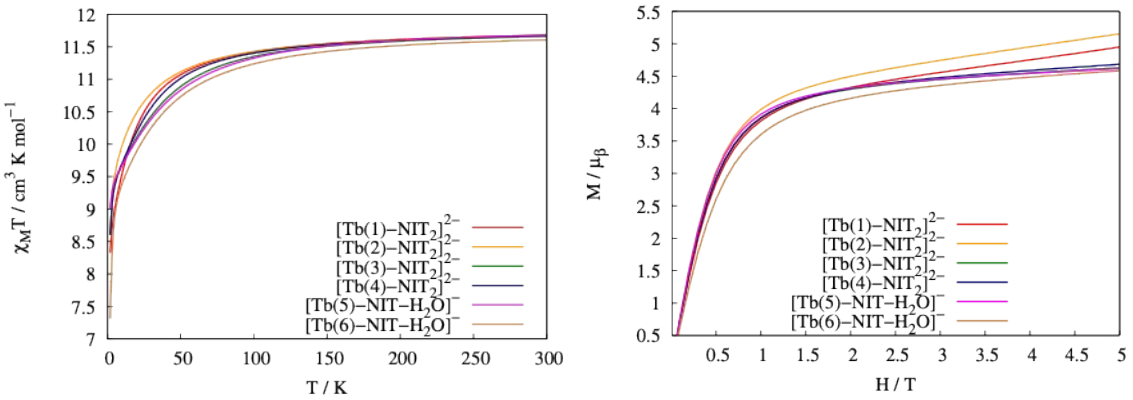

Figure S11. (left) Calculated magnetic susceptibility times temperature ($\chi_M T$, in cm^3 K mol^{-1}) as a function of T (in K) for the isolated models. (right) Calculated magnetization (M, in μ_B) as a function of the applied magnetic field (H, in Tesla) for the isolated models.

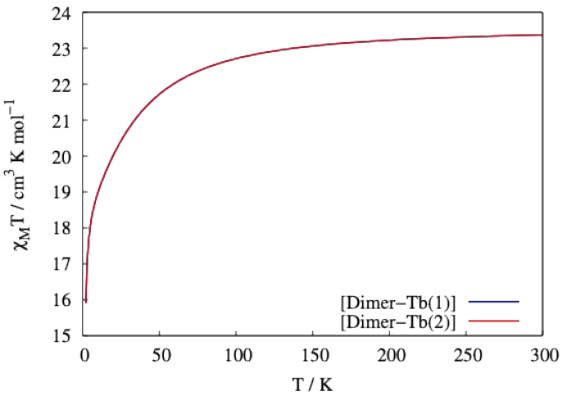

Figure S12. Calculated magnetic susceptibility times temperature ($\chi_M T$, in cm^3 K mol^{-1}) as a function of T (in K) for the dimer model.

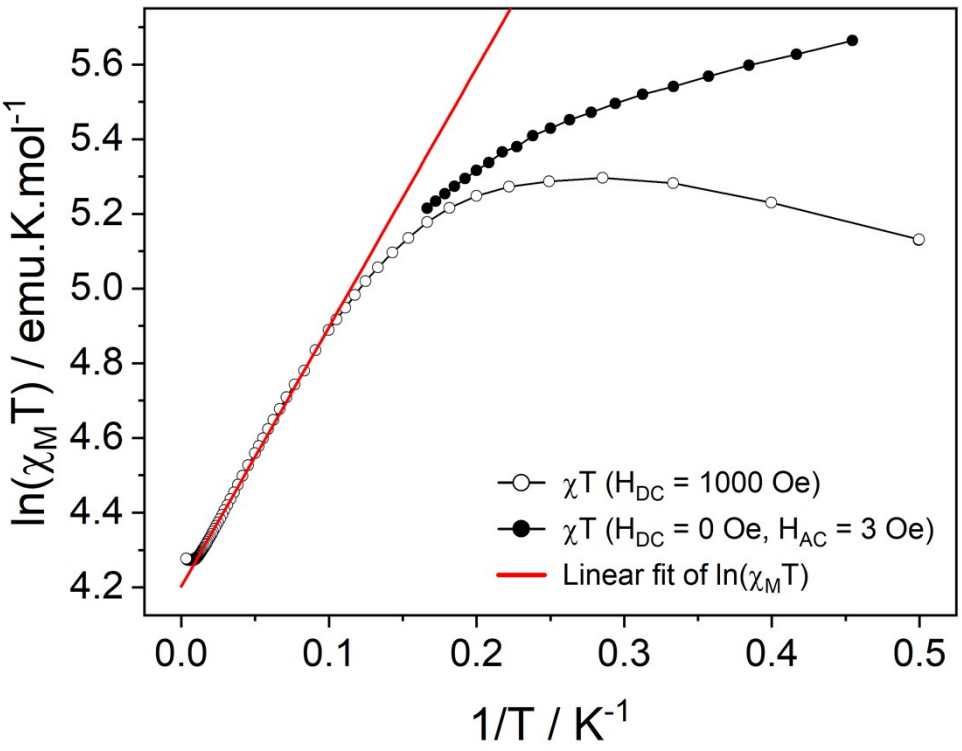

Figure S13. Reciprocal temperature dependence of ln($\chi_M T$) of *hexanuclears* with best fit as a red line ($\Delta_{\xi(dc)}$ = 6.9 ± 0.1 K, R^2 = 0.99842).

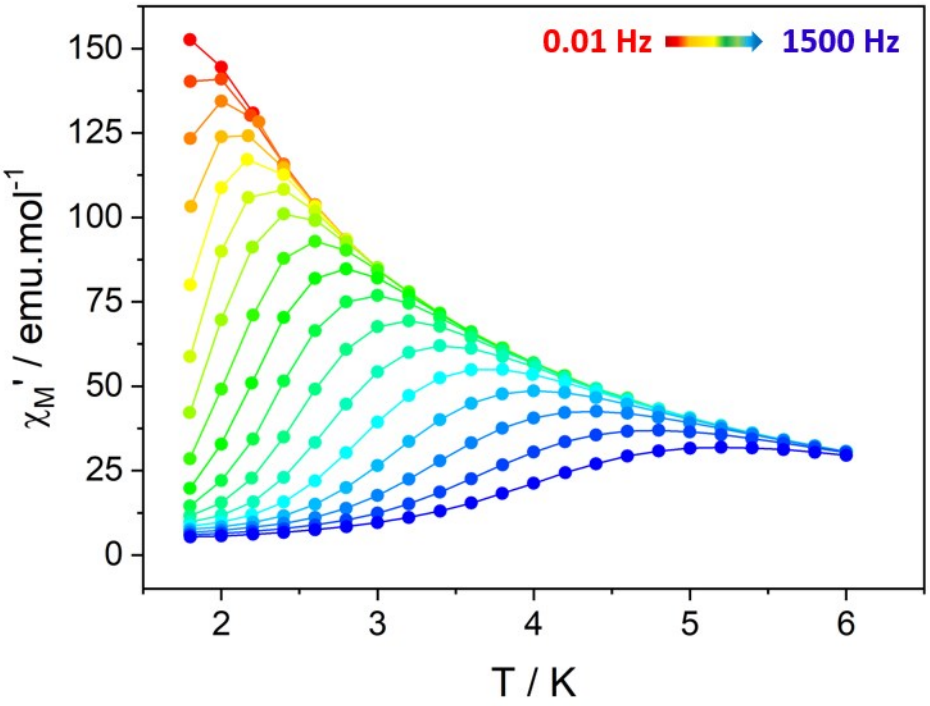

Figure S14. Temperature dependence of the in-phase component of the magnetization measured on *hexanuclears* with H_{DC} = 0 Oe between 0.01 Hz (blue) and 1500 Hz (red).

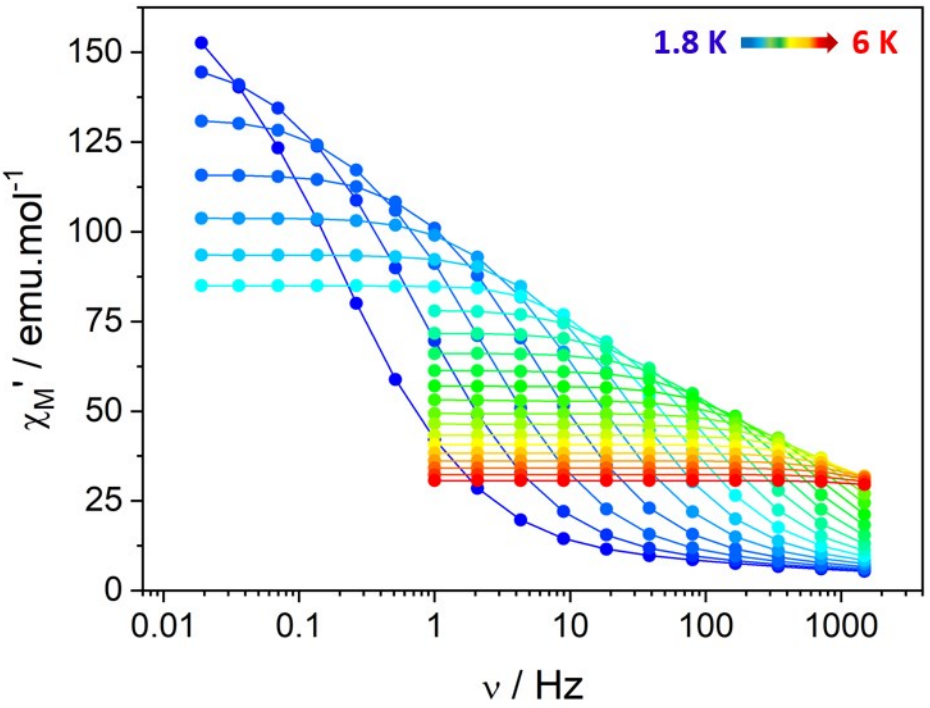

Figure S15. Frequency dependence of the in-phase component of the magnetization measured on *hexanuclears* with H_{DC} = 0 Oe between 1.8 K (blue) and 6 K (red).

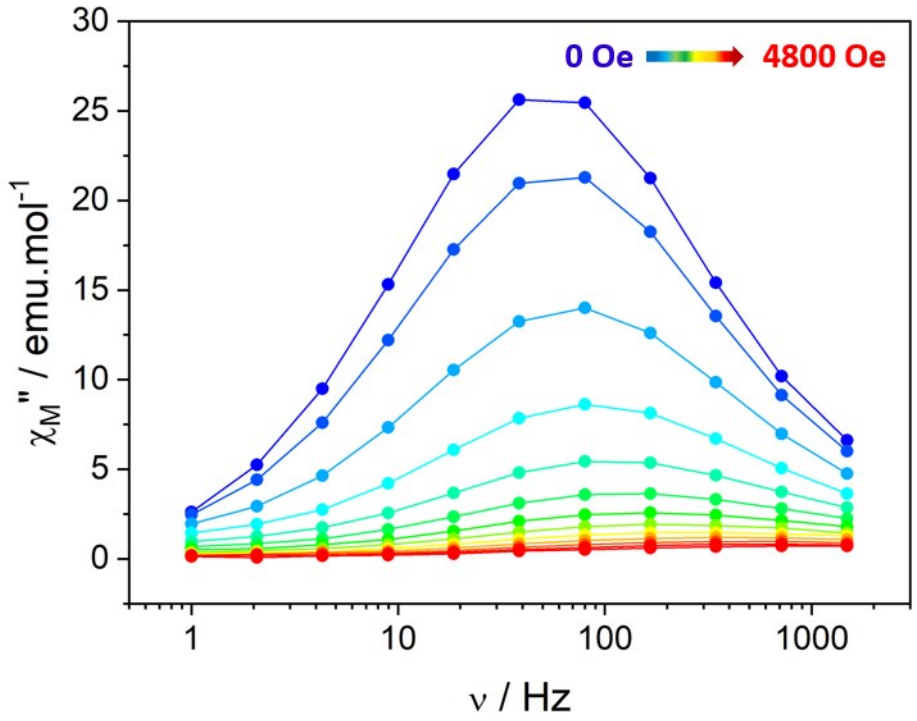

Figure S16. Field dependence of the out-of phase component of the magnetization measured on *hexanuclears* with H_{DC} = 0 Oe between 0.01 Hz (blue) and 1500 Hz (red).

Table S6. Relaxation times extracted for *hexanuclears* with H_{DC} = 0 Oe.

T (K)	τ (μs)
1.8	811019.36
2	210663.61
2.2	73890.89
2.4	26636.22
2.6	11276.34
2.8	5340.54
3	2781.21
3.2	1560.26
3.4	929.16
3.6	584.74
3.8	384.67
4.0	266.57
4.2	192.88
4.4	147.45

Table S7. Adiabatic (χ_S), isothermal (χ_T) susceptibility values and relaxation times distribution (α) extracted for *hexanuclears* with H_{DC} = 3 Oe.

T (K)	χ_S	χ_T	α	R^2
1.8	5.593	175.995	0.374	0.99817
2.0	5.518	151.472	0.346	0.99767
2.2	5.705	133.775	0.321	0.99464
2.4	5.881	117.291	0.292	0.98948
2.6	6.145	104.679	0.270	0.98739
2.8	5.903	96.078	0.278	0.99372
3.0	6.097	87.565	0.268	0.99714
3.2	6.810	79.090	0.238	0.99052
3.4	7.457	72.362	0.219	0.98996
3.6	8.336	66.532	0.199	0.99002
3.8	9.295	61.508	0.181	0.99343
4.0	10.346	57.132	0.165	0.99508

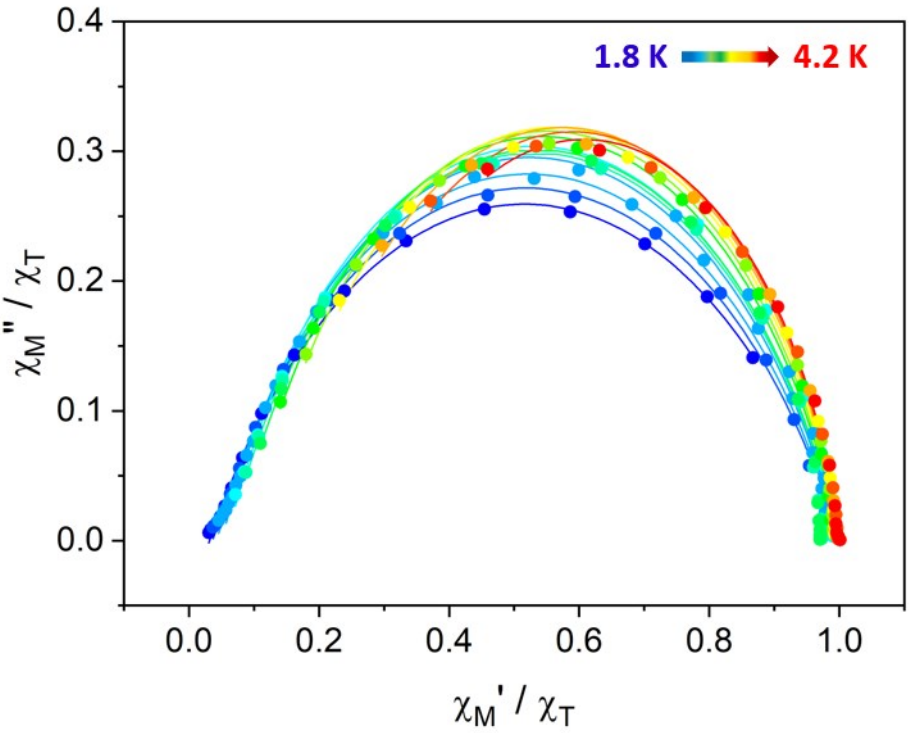

Figure S17. Normalized Argand diagram of *hexanuclears* with solid lines as best fits (Table S7).

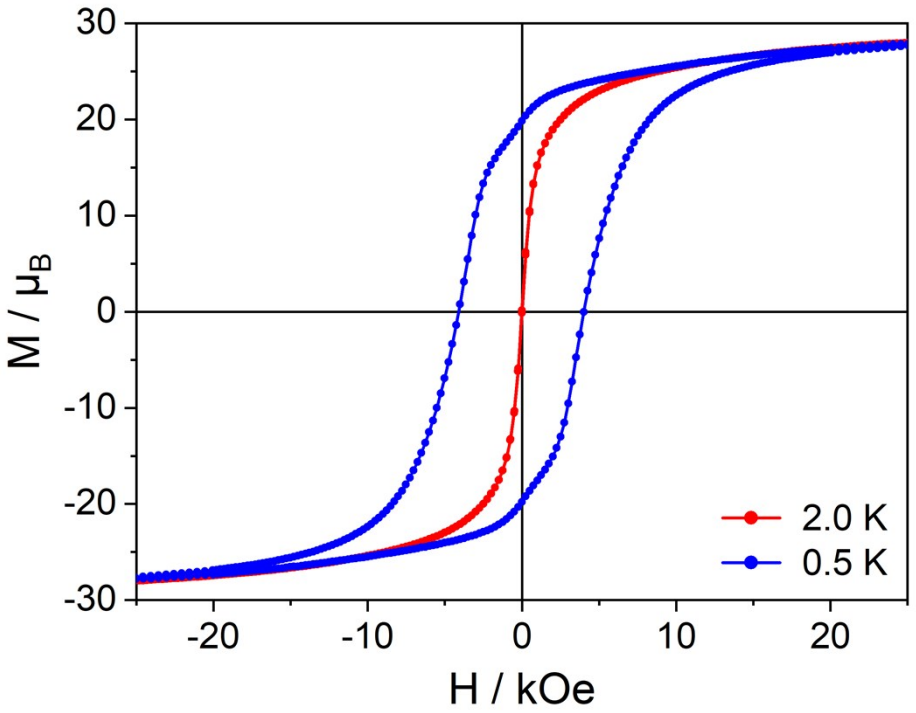

Figure S18. Hysteresis curves measured on *hexanuclears* with a 15 Oe.s^{-1} magnetic field sweep rate.

REFERENCES

[1] Sheldrick G. M.: *Acta Crystallogr. A Found. Adv.* **2015**, *71*, 3–8.
[2] Sheldrick G. M.: *Acta Crystallogr. C Struct. Chem.* **2015**, *71*, 3–8.
[3] P. van der Sluis, A. L. Spek, *Acta Crystallogr. A Found. Crystallogr.* **1990**, *46*, 194–201.
[4] A. L. Spek, *J. Appl. Crystallogr.* **2003**, *36*, 7–13.
[5] Alvarez, S.; Alemany, P.; Casanova, D.; Cirera, J.; Llunell, M.; Avnir, D.: *Coord. Chem. Rev.* **2005**, *249*, 1693-1708.
[6] te Velde, G.; Bickelhaupt, F. M.; Baerends, E. J.; Fonseca Guerra, C.; van Gisbergen, S. J. A.; Snijders, J. G.; Ziegler, T.: *Comput. Chem.* **2001**, *22*, 931-967.
[7] Fonseca Guerra, C.; Snijders, J. G.; te Velde, G.; Baerends, E. J.: *Theor. Chem. Acc.* **1998**, *99*, 391-403.
[8] Baerends, E. J.; Ziegler, T.; Atkins, A. J.; Autschbach, J.; Baseggio, O.; Bashford, D.; Bérces, A.; Bickelhaupt, F. M.; Bo, C.; Boerrigter, P. M.; Cavallo, L.; Daul, C.; Chong, D. P.; Chulhai, D. V.; Deng, L.; Dickson, R. M.; Dieterich, J. M.; Ellis, D. E.; Faassen, M. v.; Fan, L.; Fischer, T. H.; Förster, A.; Guerra, C. F.; Franchini, M.; Ghysels, A.; Giammona, A.; Gisbergen, S. J. A. v.; A. Goez; A.W. Götz; Groeneveld, J. A.; Gritsenko, O. V.; Grüning, M.; Gusarov, S.; Harris, F. E.; Hoek, P. v. d.; Hu, Z.; Jacob, C. R.; Jacobsen, H.; Jensen, L.; Joubert, L.; Kaminski, J. W.; Kessel, G. v.; König, C.; Kootstra, F.; Kovalenko, A.; Krykunov, M. V.; Lenthe, E. v.; McCormack, D. A.; Michalak, A.; Mitoraj, M.; Morton, S. M.; Neugebauer, J.; Nicu, V. P.; Noodleman, L.; Osinga, V. P.; Patchkovskii, S.; Pavanello, M.; Peeples, C. A.; Philipsen, P. H. T.; Post, D.; Pye, C. C.; Ramanantoanina, H.; Ramos, P.; Ravenek, W.; Reimann, M.; Rodríguez, J. I.; P. Ros, R. R.; Schipper, P. R. T.; Schlüns, D.; Schoot, H. v.; Schreckenbach, G.; Seldenthuis, J. S.; Seth, M.; Snijders, J. G.; Solà, M.; Stener, M.; Swart, M.; Swerhone, D.; Tognetti, V.; Velde, G. t.; Vernooijs, P.; Versluis, L.; Visscher, L.; Visser, O.; Wang, F.; Wesolowski, T. A.; Wezenbeek, E. M. v.; Wiesenekker, G.; Wolff, S. K.; Woo, T. K.; Yakovlev, A. L.: Adf 2017, Scm Teorethical Chemistry. *Vrije Univeristeit, Amsterdam, the Nederlands* **2017**.
[9] Van Lenthe, E.; Baerends, E. J.: *J. Comput. Chem.* **2003**, *24*, 1142-1156.
[10] Perdew, J. P.; Burke, K.; Ernzerhof, M.: *Phys. Rev. Lett.* **1996**, *77*, 3865-3868.
[11] Aquilante, F.; Autschbach, J.; Carlson, R. K.; Chibotaru, L. F.; Delcey, M. G.; De Vico, L.; Fernandez. Galván, I.; Ferré, N.; Frutos, L. M.; Gagliardi, L.; Garavelli, M.; Giussani, A.; Hoyer, C. E.; Li Manni, G.; Lischka, H.; Ma, D.; Malmqvist, P. Å.; Müller, T.; Nenov, A.; Olivucci, M.; Pedersen, T. B.; Peng, D.; Plasser, F.; Pritchard, B.; Reiher, M.; Rivalta, I.; Schapiro, I.; Segarra-Martí, J.; Stenrup, M.; Truhlar, D. G.; Ungur, L.; Valentini, A.; Vancoillie, S.; Veryazov, V.; Vysotskiy, V. P.; Weingart, O.; Zapata, F.; Lindh, R.: *J. Comput. Chem.* **2015**, *37*, 506-541.
[12] Roos, B. O.; Taylor, P. R.; Siegbahn, P. E. M.: *Chem.Phys.* **1980**, *48*, 157-173.
[13] Douglas, M.; Kroll, N. M.: *Annals of Physics* **1974**, *82*, 89-155.
[14] Hess, B. A.: *Physical Review A* **1985**, *32*, 756-763.
[15] Hess, B. A.: *Physical Review A* **1986**, *33*, 3742-3748.
[16] Wolf, A.; Reiher, M.; Hess, B. A.: *J. Chem. Phys.* **2002**, *117*, 9215-9226.
[17] Widmark, P. O.; Malmqvist, P. Å.; Roos, B. O.: *Theor. Chim. Acta* **1990**, *77*, 291-306.
[18] Roos, B. O.; Lindh, R.; Malmqvist, P. Å.; Veryazov, V.; Widmark, P. O.: *J. Phys. Chem. A* **2005**, *109*, 6575-6579.
[19] Roos, B. O.; Lindh, R.; Malmqvist, P.-Å.; Veryazov, V.; Widmark, P.-O.: *J. Phys. Chem. A* **2004**, *108*, 2851-2858.
[20] Malmqvist, P. Å.; Roos, B. O.; Schimmelpfennig, B.: *Chem. Phys. Lett* **2002**, *357*, 230-240.
[21] Bolvin, H.: *ChemPhysChem* **2006**, *7*, 1575-1589.
[22] hibotaru, L. F.; Ungur, L.: *J. Chem. Phys.* **2012**, *137*, 064112.